INTERFACE

rsif.royalsocietypublishing.org

Research

Cite this article: Bersi MR, Khosravi R, Wujciak AJ, Harrison DG, Humphrey JD. 2017 Differential cell-matrix mechanoadaptations and inflammation drive regional propensities to aortic fibrosis, aneurysm or dissection in hypertension. *J. R. Soc. Interface* **14**: 20170327. http://dx.doi.org/10.1098/rsif.2017.0327

Received: 5 May 2017
Accepted: 17 October 2017

Subject Category:
Life Sciences–Engineering interface

Subject Areas:
bioengineering

Keywords:
aortic stiffness, stress, inflammatory cells, angiotensin II, smooth muscle

Author for correspondence:
J. D. Humphrey
e-mail: jay.humphrey@yale.edu

Electronic supplementary material is available online at https://dx.doi.org/10.6084/m9.figshare.c.3917959.

THE ROYAL SOCIETY PUBLISHING

Differential cell-matrix mechanoadaptations and inflammation drive regional propensities to aortic fibrosis, aneurysm or dissection in hypertension

M. R. Bersi[1], R. Khosravi[1], A. J. Wujciak[1], D. G. Harrison[2,3] and J. D. Humphrey[1,4]

[1]Department of Biomedical Engineering, Yale University, New Haven, CT, USA
[2]Department of Medicine, and [3]Department of Pharmacology, Vanderbilt University, Nashville, TN, USA
[4]Vascular Biology and Therapeutics Program, Yale School of Medicine, New Haven, CT, USA

JDH, 0000-0003-1011-2025

The embryonic lineage of intramural cells, microstructural organization of the extracellular matrix, local luminal and wall geometry, and haemodynamic loads vary along the length of the aorta. Yet, it remains unclear why certain diseases manifest differentially along the aorta. Toward this end, myriad animal models provide insight into diverse disease conditions—including fibrosis, aneurysm and dissection—but inherent differences across models impede general interpretations. We examined region-specific cellular, matrix, and biomechanical changes in a single experimental model of hypertension and atherosclerosis, which commonly coexist. Our findings suggest that (i) intramural cells within the ascending aorta are unable to maintain the intrinsic material stiffness of the wall, which ultimately drives aneurysmal dilatation, (ii) a mechanical stress-initiated, inflammation-driven remodelling within the descending aorta results in excessive fibrosis, and (iii) a transient loss of adventitial collagen within the suprarenal aorta contributes to dissection propensity. Smooth muscle contractility helps to control wall stress in the infrarenal aorta, which maintains mechanical properties near homeostatic levels despite elevated blood pressure. This early mechanoadaptation of the infrarenal aorta does not preclude subsequent acceleration of neointimal formation, however. Because region-specific conditions may be interdependent, as, for example, diffuse central arterial stiffening can increase cyclic haemodynamic loads on an aneurysm that is developing proximally, there is a clear need for more systematic assessments of aortic disease progression, not simply a singular focus on a particular region or condition.

1. Introduction

The aorta is the primary conduit for blood flow and its unique structure, mechanical properties, and function play critical roles in health. Diseases of the aorta are responsible for significant morbidity and mortality, including multiple conditions (e.g. aneurysmal rupture and dissection) that lead to sudden death. Hypertension and atherosclerosis commonly coexist, and there is strong epidemiologic and experimental evidence that they exacerbate one another, particularly in conduit vessels such as the aorta. Angiotensin II (AngII) is the primary effector molecule of the renin–angiotensin system [1]. This octapeptide is a critical mediator of arterial homeostasis, but it is also fundamental in hypertensive and age-related stiffening, development of atherosclerosis, and progression of aortic aneurysms and dissections in central arteries [2,3]. Given its central role in such conditions, chronic infusion of AngII in rodents has been used widely to model ageing (low dose), atherosclerosis and hypertension (moderate dose), and aortic aneurysms and dissections (high dose) [4–7].

AngII increases blood pressure (i.e. mechanical loading) and promotes inflammation (i.e. intramural infiltration of inflammatory cells), hence it is important to define spatio-temporal interrelations between mechano- and immuno-mediated aortic remodelling in AngII infusion models of disease. Here we present the first direct comparison of evolving cell-matrix content and biaxial wall mechanics within four regions of the aorta, from proximal thoracic to distal abdominal. We use chronic infusion of AngII in atherosclerosis-prone adult male mice to induce systemic hypertension and compare spatio-temporal changes using (immuno)histological data to assess wall content and biological activity as well as *in vitro* biomechanical analyses to assess wall properties, including elastic energy storage, intrinsic material stiffness, and overall structural stiffness. The data reveal spatially distinct, time-dependent changes in cell and matrix composition and wall geometry that lead to altered biomechanical behaviours and associated regional propensities to aneurysmal dilatation, fibrotic stiffening, dissection, or short-term mechanoadaptation despite a delayed obstructive neointimal formation. Importantly, mechanical stimuli precede, and likely drive, inflammatory mediators that lead to differential regional arterial stiffening, a key indicator and initiator of diverse cardiovascular, neurovascular and renovascular diseases [8,9].

2. Material and methods

The electronic supplementary material provides detailed descriptions of all experiments and methods for image and data analysis (see electronic supplementary material, equations S1–S6) along with quantitative information, and additional discussion, on changes in tail-cuff measured blood pressures and associated spatio-temporal changes in biaxial biomechanical behaviours and immunohistological characteristics (see electronic supplementary material, figures S1–S10 and tables S1–S6). All salient findings are summarized below in Results. Unless noted otherwise, values for wall geometry, stress, stiffness and energy storage are presented at the time-specific systolic blood pressure and time- and region-specific axial stretch.

3. Results

3.1. Blood pressure elevation

Infusion of AngII at 1000 ng kg^{-1} min^{-1} for 28 days in 19.4 $\pm$ 0.2-week old, male apolipoprotein-E null (*ApoE*$^{-/-}$) mice fed a standard, low-fat laboratory diet increased systolic/diastolic blood pressures monotonically from 112 $\pm$ 4/80 $\pm$ 3 mmHg at baseline (i.e. 0 days) to 186 $\pm$ 6/141 $\pm$ 6 mmHg at 28 days ($p < 0.001$), with elevated values approaching steady state by 14 days (electronic supplementary material, figure S1 and table S1). Cessation of AngII infusion at 28 days allowed pressure to drop to 140 $\pm$ 11/107 $\pm$ 10 mmHg by 224 days, which remained elevated relative to baseline but was similar to that of non-infused age-matched mice (138 $\pm$ 5/105 $\pm$ 6 mmHg; $p > 0.05$).

3.2. General findings along the aorta

Distensibility is an often used metric of local structural stiffness [8] (electronic supplementary material, equation S6). Calculations revealed an early and sustained, significant reduction in distensibility ($p < 0.001$; figure 1*a*) in all four regions examined (electronic supplementary material, figure S2): ascending thoracic aorta (ATA), proximal descending thoracic aorta (DTA), suprarenal abdominal aorta (SAA) and infrarenal abdominal aorta (IAA). Changes at 4 days were greatest in the most proximal segment (55% reduction in ATA) and least in the most distal segment (37% reduction in IAA). Whereas distensibility tended to the same level in the ATA, DTA and SAA by 28 days of AngII infusion, the percent change remained most modest in the IAA. Given the modest-to-moderate changes in luminal diameter in all regions (electronic supplementary material, table S2), distensibility decreased primarily due to the progressive increases in blood pressure (electronic supplementary material, table S1) and associated increases in wall thickness (figures 1*b* and 2), which limits pressure-induced distensions. Increases in the thickness of the ATA and IAA tended to track the 28-day time course of blood pressure change, albeit to varying degrees. This relationship was markedly different in the DTA and SAA, where thickness tracked blood pressure over the first 14 days but increased dramatically thereafter despite the near stabilization in blood pressure. Notwithstanding the significant increases in unloaded medial thickness in three of the four regions at 28 days ($p < 0.001$; figure 2*a*,*f*–*i* and electronic supplementary material, table S4), the main contributor to the overall increase in wall thickness in the ATA, DTA and SAA was a significant increase in adventitial collagen ($p < 0.001$; figure 2*a*–*d*). Similar spatio-temporal trends were observed for the significant decreases in the *in vivo* axial stretch ($p < 0.1$ to 0.001; figure 1*c*), again most dramatic in the ATA and least so in the IAA. Differences in axial properties reveal the need to consider the wall mechanics biaxially [10,11].

Intramural cells are sensitive to changes in wall stress [12,13]. Circumferential and axial Cauchy stress-stretch data (figure 1*d*,*e* and electronic supplementary material, figure S3B) confirmed an expected early increase in wall stress due to the initial increase in blood pressure. Wall stress subsequently decreased in all regions consistent with increases in wall thickness and decreases in axial stretch (figure 1*b*,*c*); again, changes were least dramatic in the IAA. Interestingly, the percent increase in circumferential stress was highest in the SAA at 14 days (68%) whereas it peaked at lower percent increases (<50%) at 4 days in the other three regions. The eventual reduction in circumferential stress resulted in values well below normal in the ATA and especially in the DTA ($p < 0.05$) and SAA, with the latter two reductions manifesting abruptly at 21 days consistent with the dramatic pressure-independent increase in wall thickness. The time course of changes in axial stress was similar to that of circumferential stress across the four regions: monotonic changes in the ATA, little change in the IAA and slight increases followed by abrupt decreases in the DTA and SAA.

3.3. Ascending thoracic aorta (ATA)

A key mechanical function of large arteries is to store elastic energy during systole and to use this energy to work on the blood during diastole to augment blood flow [14,15]. In contrast to the initially rapid loss of distensibility (recall figure 1*a*), elastic energy storage decreased more slowly in the ATA, reaching an apparently new steady-state value within 14 days that was significantly lower than baseline ($p < 0.001$; figure 1*h* and electronic supplementary material, figure S9), the same period over which blood pressure reached its near steady state (electronic supplementary

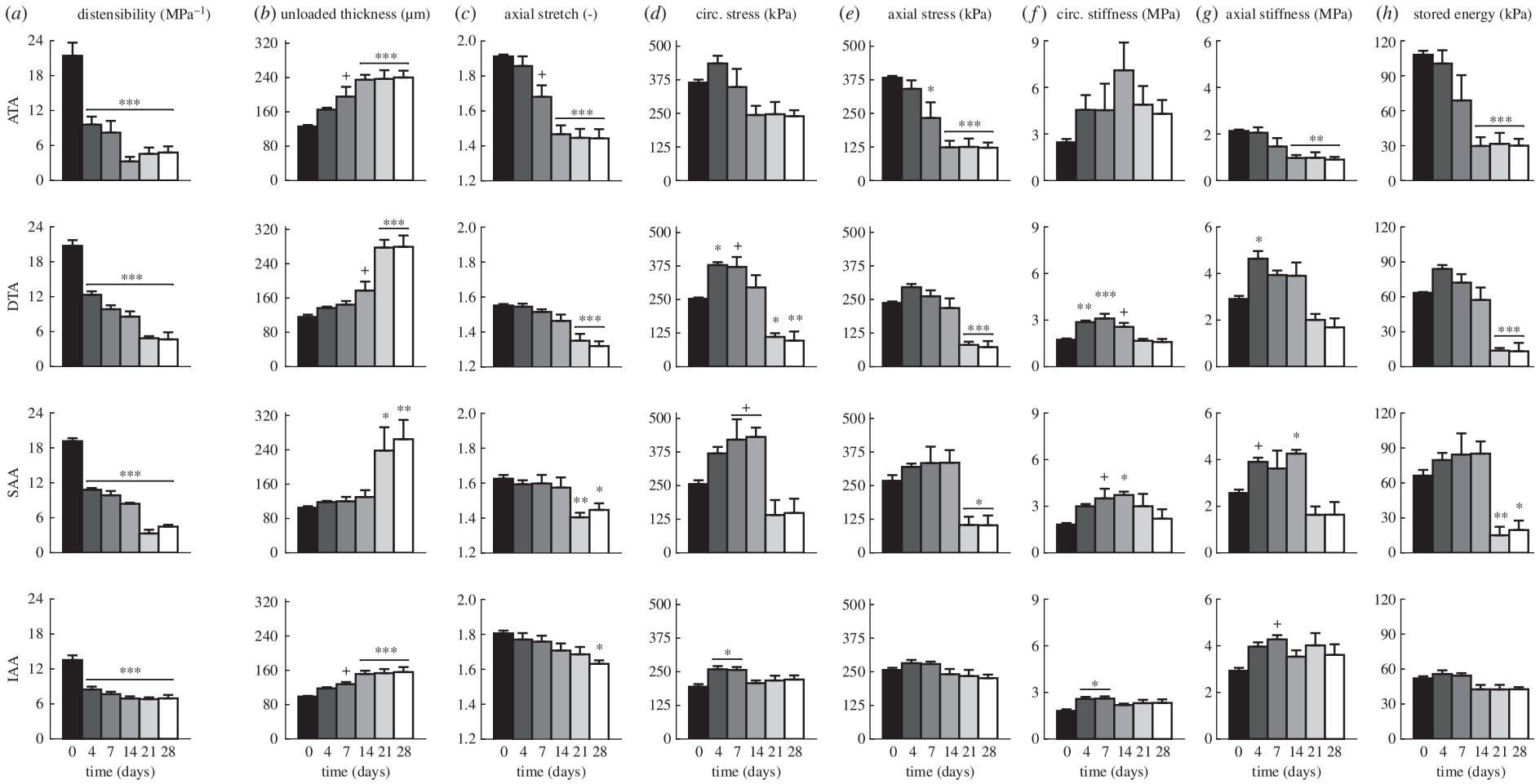

Figure 1. Spatio-temporal differences in geometric, material and structural properties. Mean ± s.e.m. values of (*a*) distensibility MPa^{-1}, (*b*) unloaded wall thickness (μm), (*c*) axial stretch, (*d,e*) circumferential and axial stress (kPa), (*f,g*) circumferential and axial stiffness (MPa) and (*h*) stored energy (kPa) from four aortic regions (ATA, DTA, SAA, IAA; see electronic supplementary material, figure S2) at six times throughout AngII infusion: baseline (0 days), 4, 7, 14, 21 and 28 days ($n = 4–7$ samples per group). Significant differences from baseline (0 days) denoted by $^{+}$, *, **, *** $p < 0.1, 0.05, 0.01, 0.001$. Values for all metrics are in electronic supplementary material, table S2 and were computed at time-specific systolic pressures (electronic supplementary material, table S1), unless otherwise indicated. Note, in particular, the distinctive time course of changes in circumferential material stiffness in the ATA and circumferential stress in the SAA, with the most dramatic late thickening of the wall in the DTA and the modest changes overall in the IAA.

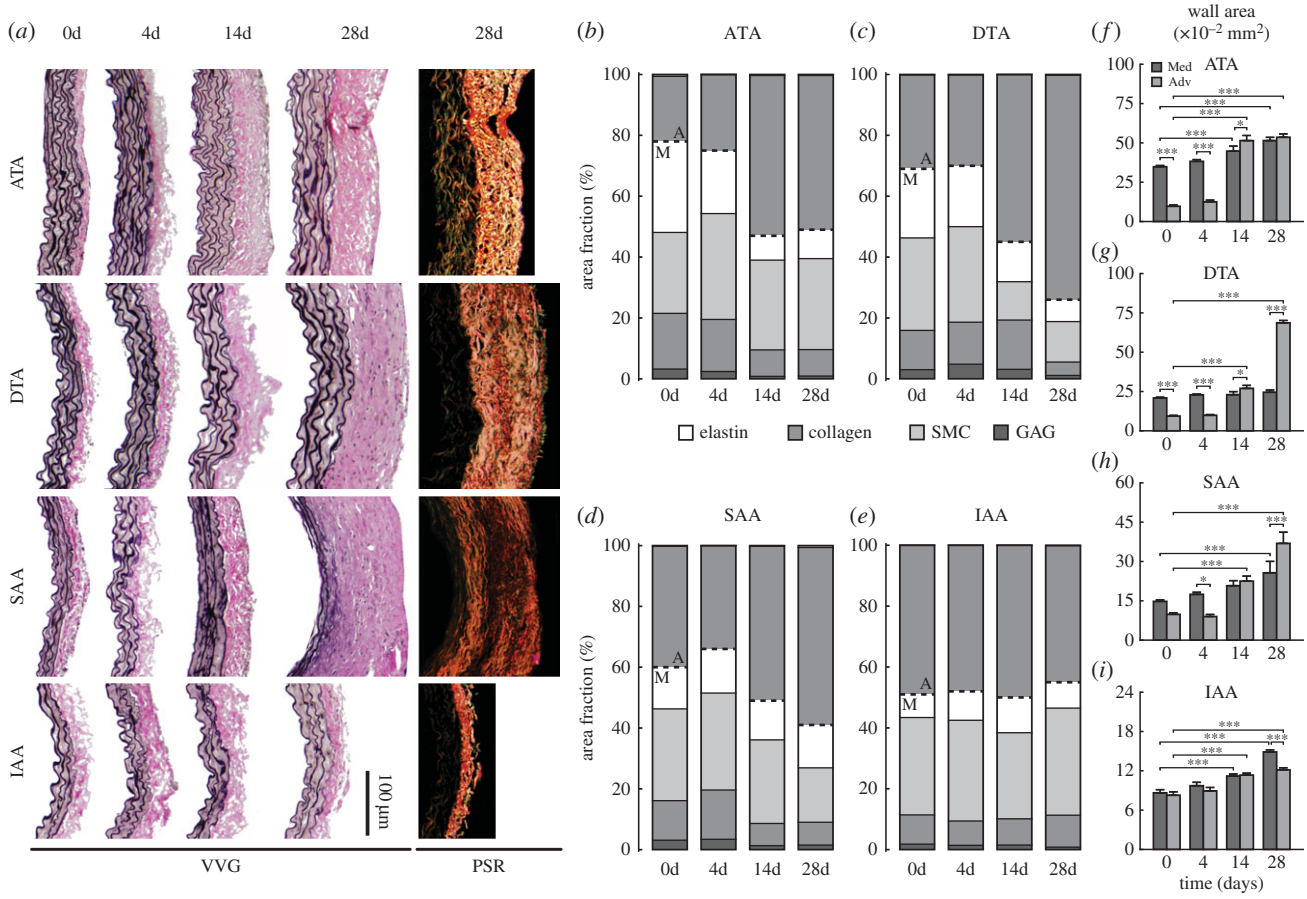

Figure 2. Spatio-temporal differences in wall composition and structure. (*a*) Representative VVG stained histological sections show wall thickness and elastin (black) from four aortic regions (ATA, DTA, SAA, IAA) at four times throughout AngII infusion: baseline (0 days), 4, 14 and 28 days. PSR staining at 28 days reveals excessive adventitial collagen deposition in three of the four regions, but especially the DTA. Quantification of layer-specific (medial—M, below dashed line and adventitial—A, above dashed line) constituent area fractions—elastin (white), collagen (medium grey), smooth muscle (SMC; light grey) and glycosaminoglycans (GAG; dark grey)—are shown for the (*b*) ATA, (*c*) DTA, (*d*) SAA and (*e*) IAA. Despite differences in elastin, collagen and SMCs, changes in GAGs were unremarkable. (*f–i*) Layer-specific values (mean ± s.e.m.) for cross-sectional areas from the same four regions and times are delineated for the media (dark grey) and adventitia (medium grey) ($n = 10$ images per group). The adventitial percentage and area increased by 28 days in all regions except the IAA. Overbar denotes statistical significance between groups, where *, **, ***$p < 0.05$, 0.01, 0.001. Values for all metrics are in electronic supplementary material, tables S4 and S5.

material, figure S1). Whereas distensibility, stored energy and axial stiffness (figure 1*g*) all decreased nearly monotonically over the 28 days of AngII infusion, notwithstanding greater specimen-to-specimen variability the circumferential material stiffness (figure 1*f*) increased dramatically over the first 14 days (2.9-fold higher on average), then decreased though not recovering its original level (remaining 1.8-fold higher at 28 days). Interestingly, the modest reductions in circumferential stiffness occurred after day 14 despite the nearly constant blood pressure (electronic supplementary material, figure S1) and wall thickness (figure 1*b*, electronic supplementary material, table S2A). Recalling that wall thickness increased due to both an early expansion of the media and a later extensive deposition of collagen in the adventitia (figure 2*a,b,f* and electronic supplementary material, figure S5, tables S4 and S5A), immunohistochemistry yet revealed early increases, by day 4, in MMP-2 and -13 (a gelatinase and collagenase, respectively, that can degrade collagen fibres), which persisted in the media and adventitia through day 28; delayed (up to day 14) adventitial increases in MMP-12 (an elastase) also persisted to day 28 (figure 3*a–c* and electronic supplementary material, figure S7 and table S5A). By day 14, the media often exhibited many sites of focal breakage of elastic laminae (electronic supplementary material, figure S6) consistent with degeneration of the medial layer and loss of mechanical integrity [16], both of which can lead to aneurysmal dilatation.

3.4. Descending thoracic aorta (DTA)

Unlike its ascending counterpart, the DTA exhibited an early increase in elastic energy storage followed by a gradual return to normal by 14 days, then a precipitous drop (79% reduction) to levels significantly below normal by 21–28 days ($p < 0.001$; figure 1*h*). Histological examination of the DTA failed to reveal either breakage of elastic laminae or focal medial degeneration as in the ATA (electronic supplementary material, figure S6), consistent with the lack of dilatation. Immunohistological analysis revealed a transient but non-significant increase, at day 4, in MMP-13 (figure 3*c*), suggesting an early increased potential for collagen degradation. The intrinsic circumferential stiffness increased slightly over the first 4 to 7 days, likely due to pressure-induced stretching of extant collagen fibres, but this stiffness decreased by 21 days to a level close to baseline (figure 1*f*). Axial stiffness similarly increased and then decreased, albeit to a persistently lower level than baseline (figure 1*g*), consistent with a delayed reduction in axial stretch (figure 1*c*). These non-monotonic changes in energy

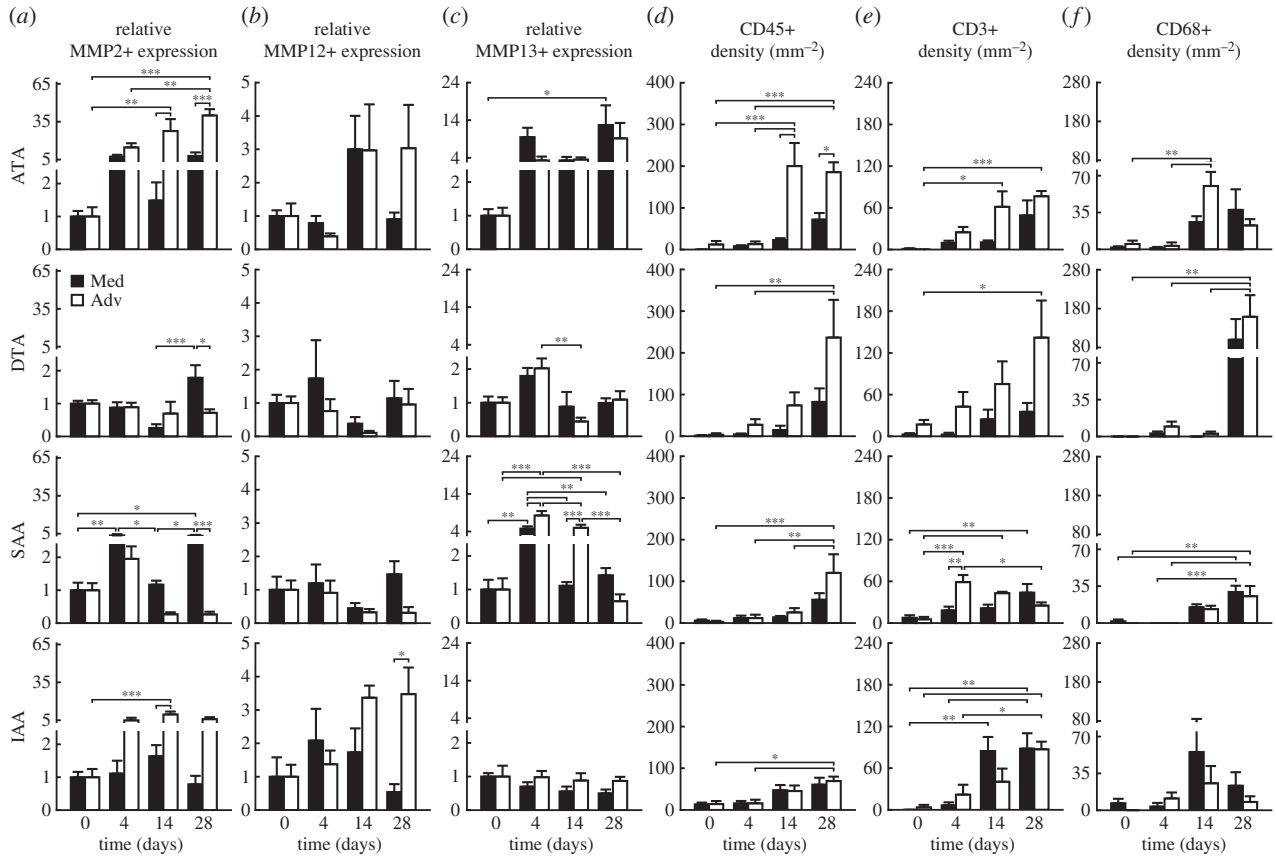

Figure 3. Spatio-temporal differences in matrix metalloproteinases and inflammatory cells. Mean ± s.e.m. values, relative to baseline, for (*a*) MMP-2, (*b*) MMP-12 and (*c*) MMP-13 expression, and (*d*) $CD45^+$, (*e*) $CD3^+$, and (*f*) $CD68^+$ cell density (per mm^2) from four aortic regions at four times throughout AngII infusion: baseline (0 days), 4, 14 and 28 days ($n = 6$ images per group). Layer-specific content is reported separately for the media (black bar) and adventitia (white bar). Overbar denotes statistical significance between groups, where *, **, ***$p < 0.05$, 0.01, 0.001. Values for all metrics are in electronic supplementary material, table S5.

storage and biaxial stiffness occurred while thickness initially increased progressively, then abruptly at day 21 (figures 1*b*, 2*a*,*c*, electronic supplementary material, table S2B). Although qualitatively similar to the predominant adventitial thickening of the ATA, the relative thickening of the DTA was greater (2.4 fold versus 1.9 fold in ATA), again driven by a dramatic increase in adventitial collagen (figure 2*a*,*c*,*g* and electronic supplementary material, figure S5B). Toward this end, MMP-2, -12 and -13 activity was not significantly different from day 14 to 28 (figure 3*a*–*c*, electronic supplementary material, table S5B), suggesting an increased deposition of matrix without concomitant degradation.

3.5. Suprarenal abdominal aorta (SAA)

Like the DTA, the SAA experienced an early increase in stored energy (figure 1*h*), albeit one that persisted over the 14 days that blood pressure increased (electronic supplementary material, figure S1), prior to decreasing abruptly at 21 days (70% reduction) and remaining significantly lower than baseline through 28 days ($p < 0.05$ to 0.01; figure 1*h*). This observation paralleled the abrupt increase in wall thickness and decrease in axial stretch at 21 days (figure 1*b*,*c*). Interestingly, circumferential material stiffness increased over the first 14 days, while pressure increased, then returned toward baseline at 28 days (figure 1*f*) while pressure remained nearly the same (electronic supplementary material, figure S1). Axial stiffness also increased over the first 14 days, then decreased to a value just lower than baseline (figure 1*g*). The SAA alone showed a slight early reduction (at day 4) in the percentage of the wall occupied by the adventitia (figure 2*d*, electronic supplementary material, table S4), consistent with a peak in MMP-13 activity and high medial MMP-2 expression after day 4 (figure 3*a*–*c*, electronic supplementary material, table S5C). This initial decrease was followed by an increase in adventitial thickness due to considerable collagen deposition (figure 2*a*,*d*,*h* and electronic supplementary material, figure S5B).

3.6. Infrarenal abdominal aorta (IAA)

Despite an early decrease in distensibility (figure 1*a*), likely due to the increases in pressure (electronic supplementary material, figure S1) and wall thickness (figure 1*b*), the IAA exhibited the least biomechanical changes of the four regions. There were modest changes in biaxial stress (figure 1*d*,*e* and electronic supplementary material, figure S3B), elastic energy storage (figure 1*h* and and electronic supplementary material, figure S9) and circumferential material stiffness (figure 1*f*), with only a slight increase in axial material stiffness (figure 1*g*) that may have offset the gradual progressive decrease in axial stretch (figure 1*c*). These modest changes were consistent with a minimal change in wall composition (figure 2*a*,*e*) and overall geometry (electronic supplementary material, table S2D). Importantly, MMP-13 did not change over the 28-day period, though MMP-2 and -12 increased and remained elevated in the adventitia (figure 3*a*–*c*, electronic supplementary material, table S5D). Whereas the DTA experienced marked adventitial thickening in the absence of elevated MMP levels (i.e. deposition >

degradation), increased MMP-2 expression in the IAA may have mediated the marginal adventitial changes due to an increased potential to turnover matrix (deposition ≅ degradation). Finally, note that the baseline distensibility (figure 1*a*) and elastic energy storage (figure 1*h*) were lowest in the IAA, consistent with its more distal location and reduced elastic fibre content (figure 2*a*,*e* and electronic supplementary material, figure S5, table S5D), yet its evolving biaxial stiffness was comparable to the DTA and SAA. Best-fit values of material parameters used to compute all relevant material metrics for each time and region are given in electronic supplementary material, table S3.

3.7. Inflammatory infiltrates

Mechanical stress can promote the deposition and degradation of matrix by intramural cells, the latter primarily via MMP production and activation [17,18]. Mechanical stress can also promote the expression of diverse chemokines (e.g. MCP-1) and cytokines (e.g. TGFβ) that can influence inflammatory cell recruitment and activity [13,19]. Baseline numbers of $CD45^+$(a pan-inflammatory leukocyte marker) cells were low in all four regions, but differentially increased over the 28 days of AngII infusion (figure 3*d* and electronic supplementary material, figure S7B and table S5). Consistent with the aforementioned compositional and mechanical findings, significant increases in $CD45^+$ cells occurred earliest in the ATA and then in the DTA and SAA ($p < 0.01$ to 0.001), with the smallest changes in the IAA ($p < 0.05$). Indeed, the consistently high levels of $CD45^+$ cells from 14 to 28 days in the ATA (figure 3*d*, electronic supplementary material, table S5A) mirrors the constancy over this period in wall thickness and axial stretch (figure 1*b*,*c*), biaxial wall stress (figure 1*d*,*e*) and stored energy and axial stiffness (figure 1*g*,*h*). Relative CD45 expression was far greater in the adventitia than in the media in the ATA, DTA and SAA, particularly on or after day 14, consistent with the preferential thickening of the adventitia in these regions (figure 2*a*–*d*,*f*–*h*). While the IAA experienced less change in wall thickness relative to other regions, histological inspection revealed a modest thickening in both the medial and adventitial layers (figure 2*a*,*i*, tables S2D and S4), consistent with the near uniform low density of $CD45^+$ cells (figure 3*d*, electronic supplementary material, table S5D). The presence of $CD3^+$ cells (a T-cell marker; figure 3*e* and electronic supplementary material, figure S7A) tracked the presence of $CD45^+$ cells in the ATA and DTA, consistent with prior observations [20]; $CD3^+$ cell density was also highest in the adventitia of the DTA at 28 days, consistent with the greatest collagen deposition of any region at any time (cf. figure 2*a*,*c*,*g*). Finally, baseline numbers of $CD68^+$ cells (a macrophage marker; figure 3*f* and electronic supplementary material, figure S7C) were also low in all regions, but increased by day 14 in the ATA and especially by day 28 in the DTA and SAA. Temporal changes in circumferential stiffness did not track those for inflammatory infiltrates in any region.

3.8. Mechanoinflammatory correlates

Given the multiple cell types and MMPs considered as well as the many mechanical metrics, we computed Pearson product–moment correlations amongst 16 variables of interest (i.e. two mechanical stimuli—mean and pulse pressure, six biological responses—expression of three inflammatory cell markers and three MMPs, and eight mechanical consequences—metrics of material behaviour) for (i) data pooled from the four regions along the aorta (electronic supplementary material, figure S10A), (ii) data grouped by thoracic (ATA, DTA) or abdominal (SAA, IAA) segment (figure 4*a*,*b*) and (iii) data for the four individual regions (electronic supplementary material, figure S10F–I). Notwithstanding differences between the ATA and DTA and between the SAA and IAA (figure 1, electronic supplementary material, table S2), comparisons between thoracic and abdominal segments were informative. For example, most metrics that correlated with increased pressure, correlated better with pulse than mean pressure, consistent with a prior finding using a different model of induced hypertension [22]. The thoracic aorta tended to have stronger correlations between wall mechanics and inflammation than did the abdominal aorta. Namely, whereas inflammatory cells correlated positively with blood pressure ($p < 0.01$) and wall remodelling (thickness; $p < 0.01$) and negatively with multiple metrics of aortic function (stored energy, biaxial stress; $p < 0.05$) in the thoracic aorta, the strength and significance of these correlations was less in the abdominal aorta (figure 4*a*,*b*). Importantly, independent of region, overall wall thickness had a strong positive correlation with $CD45^+$ cells ($p < 0.01$) while energy storage had a strong negative correlation ($p < 0.05$), indicating consistent relationships between inflammatory burden and wall remodelling leading to a loss of aortic function. Recalling that circumferential stiffness was maintained at or restored to near baseline values in all regions except the ATA (figure 1*f*), it was not surprising that this metric did not correlate with any inflammatory indicator and thus may be controlled mainly by mechanosensing or mechanoregulation of the extracellular matrix [23].

3.9. Long-term responses along the aorta

Many of our AngII infused mice (>60%) presented with a thoracic aneurysm, a stable dissection of the SAA, or sudden death due to a ruptured lesion within 28 days; affected regions from these mice were excluded from this study as we focused on biomechanical propensity to disease (hence the regular, low-fat diet). Note, however, that three mice presenting with a stable SAA dissection at euthanasia (figure 5) were studied for approximately 7 months following the 28-day infusion with AngII (224 days post-surgery) to assess the potential for either reverse remodelling or continued disease progression. Long-term findings for the ATA, DTA and IAA were compared with vessels harvested at baseline, immediately following AngII infusion for 28 days, or after approximately 1 year of age (age-matched) without any history of AngII infusion (224d no AngII; figure 5*a*–*h*).

The previously treated ATA (224d, figure 5) showed a persistent long-term elevation in circumferential material stiffness (approx. 2.9-fold at systolic pressure) at a level similar to that which evolves in this region with normal ageing up to approximately 1 year (224d no AngII; figure 5*e*). The long-term, previously treated ATA also had values of axial stretch, axial stiffness, circumferential and axial stress and energy storage that differed little from the 28-day infusion group ($p > 0.05$ versus 28 days for all metrics; figure 5) and thus were markedly reduced relative to the young control ($p < 0.05$ or $p < 0.001$ versus 0 d; figure 5*b*–*d*,*f*,*h*). Although natural ageing to approximately 1 year resulted in significantly decreased axial stretch, axial stress and energy storage ($p < 0.05$

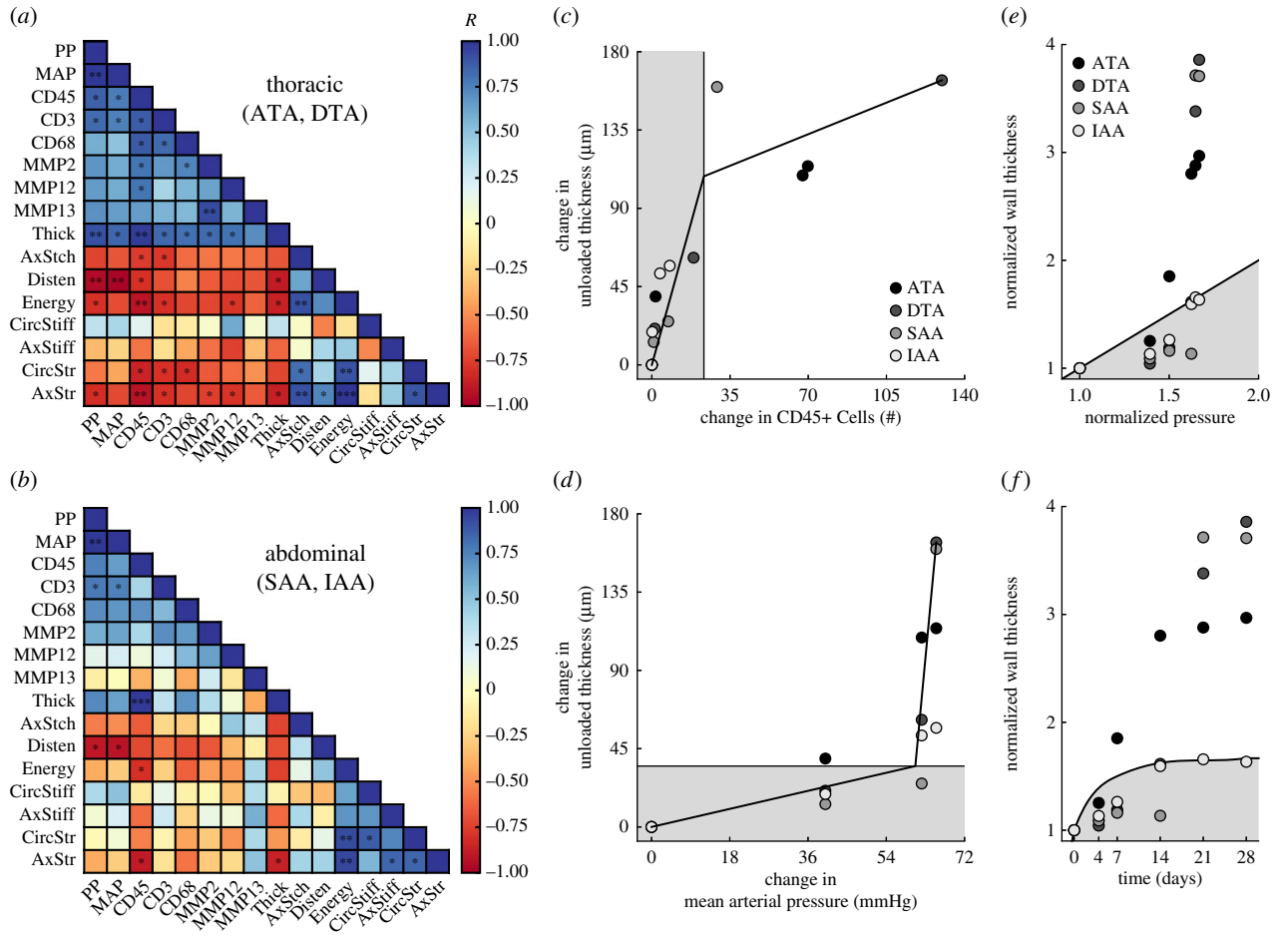

Figure 4. Mechano-inflammatory correlates reveal a distinct time course of remodelling. Heat maps of the Pearson correlation coefficient R for pooled (*a*) thoracic and (*b*) abdominal segments ($n = 8$ points per correlation); blue indicates a positive and red a negative correlation. Piecewise linear fitting of the change in wall thickness versus the change in (*c*) $CD45^+$ cells or (*d*) mean arterial pressure for all regions and times reveals an early mechano-mediated remodelling (grey region) followed by a later inflammatory-mediated remodelling (white region). Mechanoadaptation is defined by a linear relationship between normalized changes in pressure and wall thickness (i.e. $\gamma = P_{sys}/P_{sys}^{0d} = h/h^{0d}$) [21]. The time course of thickness adaptation should, therefore, mimic the nearly logarithmic behaviour of the pressure increase (cf. electronic supplementary material, figure S1). (*e*) Pressure- and (*f*) time-dependent thickness adaptation was achieved by the IAA alone (light grey circles). Data off the line of identity (black line in *e*), or the line of adaptation (black curve in *f*), indicate areas of either progressively adaptive ($\gamma > h/h^{0d}$; grey) or maladaptive ($\gamma < h/h^{0d}$; white) remodelling. Statistical significance (in *a* and *b*) is denoted by *, **, ***$p < 0.05$, 0.01, 0.001. All correlation coefficients and *p*-values are in electronic supplementary material, tables S6A–N.

versus 0d; figure 5*b*,*d*,*h*), these reductions from baseline were much less than those in the AngII infused groups ($p < 0.001$ versus 0d). Indeed, ageing alone did not affect circumferential stress or axial stiffness primarily because of the modest effect on the unloaded thickness ($p > 0.05$ versus 0d; figure 5*a*,*c*,*f*). Of course, given the long half-life of vascular elastin, one should not expect ageing (with little to no natural elastic fibre degradation) to reduce energy storage to levels similar to those in cases of pathological elastic fibre fragmentation (cf. electronic supplementary material, figure S6). While wall thickness was similar among AngII infused groups, histological analysis revealed changes in wall composition (electronic supplementary material, figure S5A). In particular, by 224 days, an average ATA cross-section contained 11% neointima and 27% adventitia, a marked reduction from 51% adventitia at 28 days (figure 5*i*,*m*, electronic supplementary material, table S4).

In contrast, the previously treated DTA showed persistent values of circumferential stiffness at a level slightly lower than both the 0 and 224 day controls ($p < 0.01$ versus 224d no AngII; figure 5*e*). The lower values of axial stretch and stiffness, circumferential and axial stress and energy storage that resulted from 28-day infusion with AngII ($p < 0.05$ or $p < 0.001$ versus 0d; figure 5*b–d*, *f–h*) improved only slightly over the 7-month recovery period, driven primarily by a modest reduction in unloaded wall thickness (from 279 to 232 μm; figure 5*a*, electronic supplementary material, table S2B). This reduction in thickness appeared to result from a reduced adventitial wall percentage (74% at 28 days versus 45% at 224 days; figure 5*j*,*n*, electronic supplementary material, table S4), which appeared sufficient to improve distensibility ($p < 0.01$ versus 28d; figure 5*g*) and increase biaxial stress and stored energy slightly (figure 5*c*,*d*,*h*), though not to baseline levels. Interestingly, ageing alone did not affect any of the mechanical metrics in either the DTA or IAA, save a modest decrease in distensibility ($p < 0.001$ and $p < 0.05$ versus 0 days in the DTA and IAA, respectively; figure 5*g*) and a slight increase in axial stiffness ($p > 0.05$ for both regions; figure 5*f*).

In stark contrast, despite showing modest compositional or biomechanical changes over 28 days of AngII infusion (cf. figures 1 and 2), the IAA developed a marked neointimal thickening (figure 5) that was nearly occlusive, occupying 57%, on average, of the total wall cross-sectional area by

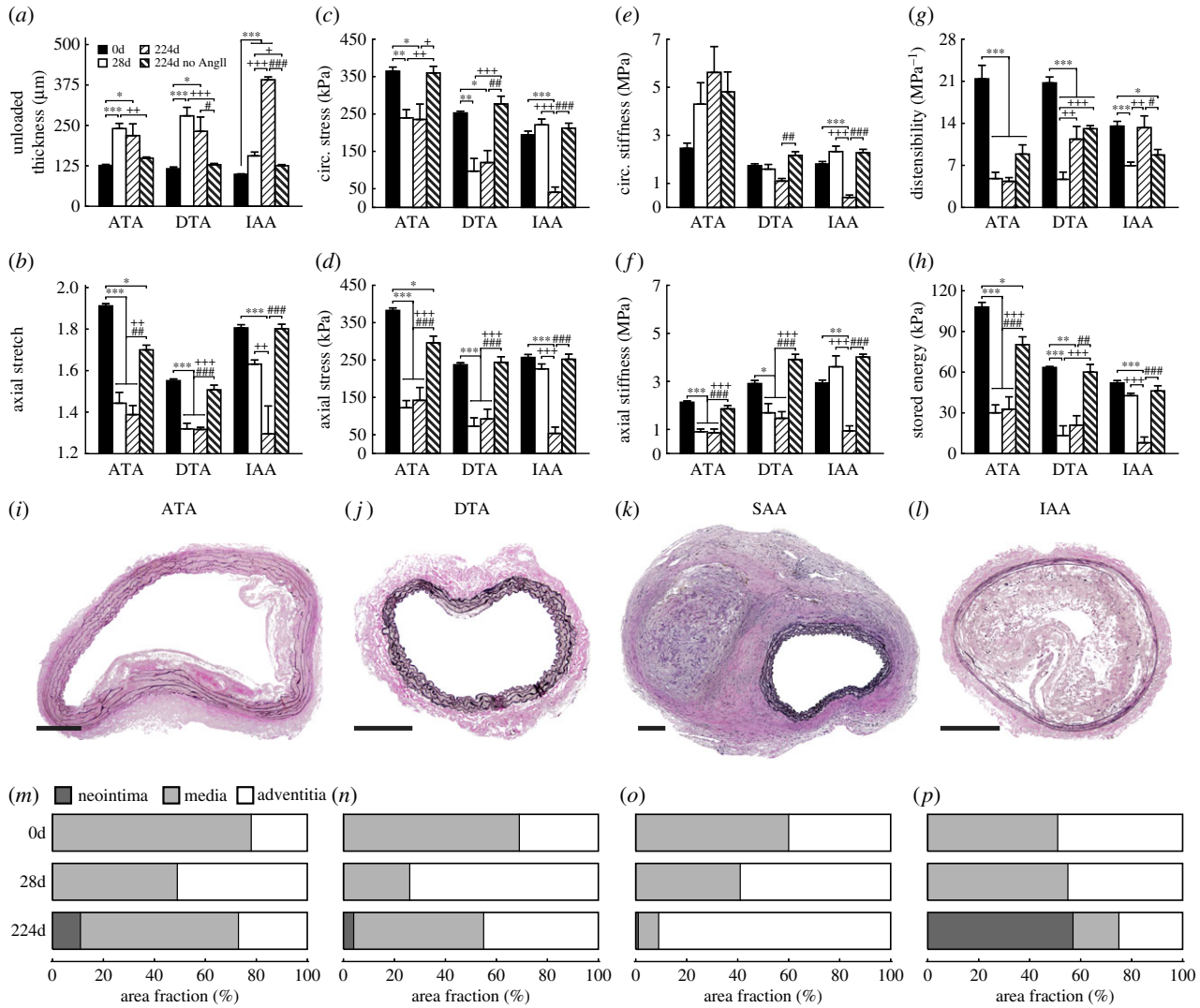

Figure 5. Long-term regional differences in geometric, material and structural properties. Mean ± s.e.m. values of (*a*) unloaded wall thickness, (*b*) axial stretch, (*c,d*) circumferential and axial stress, (*e,f*) circumferential and axial stiffness, (*g*) distensibility and (*h*) stored energy from three aortic regions at four times: baseline (0d), 28 days of AngII infusion (28d), 28 days of AngII infusion followed by 196 days of no infusion (224d) and age-matched controls at 224 days without any AngII infusion (224d no AngII); $n = 3$ to 7 per group. Representative VVG stained sections from the (*i*) ATA, (*j*) DTA, (*k*) SAA and (*l*) IAA reveal variations in cross-sectional layer composition; mean values for each group are shown in (*m–p*). Note that images are representative for the 224d group only as samples with advanced disease (as in the SAA) have been excluded from all prior analyses. Scale bars represent 250 μm. Overbars denote statistical significance, where *, **, ***$p < 0.05$, 0.01, 0.001 and *, $^{+}$ and $^{\#}$ denote differences versus 0, 28 and 224 days, respectively. Values for all metrics are in electronic supplementary material, tables S2 and S4.

224 days (figure 5*l,p* and electronic supplementary material, figure S5H–L and table S4). For this reason, the computed mechanical metrics for the previously treated IAA at 224 days (figure 5*c–h*, electronic supplementary material, table S2D) should be interpreted with caution, if at all, noting that there were only modest changes in three of the metrics with normal ageing of the IAA: decreased distensibility ($p < 0.05$ versus 0d; figure 5*g*) and increased biaxial stiffness ($p > 0.05$ versus 0d; figure 5*e,f*).

4. Discussion

Pressure-induced increases in aortic wall stress stimulate a local production of both AngII, which associates with increases in TGFβ and promotes matrix deposition [17,24], and MMPs, which drive matrix degradation [18,25]. Elevating pressure with exogenous AngII can exacerbate both responses, though not necessarily equally. It is, of course, the ratio between deposition and degradation that largely dictates whether a local biomechanical response is homeostatic or pathologic [26,27]. This study shows, in adult male *ApoE*$^{-/-}$ mice, that the time courses, types and extents of biomechanical responses to the same chronic AngII stimulus differ significantly across aortic regions (figures 1 and 2 and electronic supplementary material, figure S5), leading to a propensity to aneurysmal dilatation (ATA) [16], a marked structural stiffening via excessive fibrosis (DTA) [20], a propensity to dissection (SAA) [4] or an early homeostatic response followed by a marked long-term neointimal development (IAA). Notwithstanding possible haemodynamically driven regional differences in pulse pressure, it was remarkable that such different disease processes manifested within a single hypertensive model.

High-dose AngII infusion in *ApoE*$^{-/-}$ mice is widely used to study the pathology of aortic dissections, which occur almost exclusively in the SAA in these mice [4,28,29] (in contrast to humans wherein dissections manifest in the thoracic

aorta). Two distinctive biomechanical features manifested in this region—biaxial wall stress and energy storage continued to increase over the first 14 days (figure 1*d*,*e*,*h*). Since functional elastic fibres are not produced in maturity [14], this transient increase in energy storage implies a greater deformation of the elastic fibres at 4+ days, which could occur via an increase in pressure, a reduction in the constraining fibrillar collagens, or both. Noting that suprarenal aortic dissection typically occurs within 3–10 days after starting AngII infusion [28], the continued increases in these mechanical metrics suggests a delayed deposition of the collagen that is needed to stress shield the media during this period of increasing pressure (electronic supplementary material, figure S1 and table S1) and increased MMP activity (figure 3, electronic supplementary material, table S5). Indeed, the SAA experienced the smallest early increase in wall thickness (figures 1*b* and 2, electronic supplementary material, table S2C) and it alone saw a reduction at day 4 in the percentage of wall occupied by adventitia (figure 2*d*, electronic supplementary material, table S4), consistent with increased levels of MMPs (figure 3*a*,*c*, electronic supplementary material, table S5C). That $CD68^+$ cells were not increased during this vulnerable period likely reflects the selection bias in that we only studied vessels that had not dissected at the time of tissue harvest; SAAs at 4 and possibly 7 days could have gone on to dissect if left *in vivo*, whereas those at 14–28 days would likely not have dissected if left *in vivo*. We expect early increases in energy storage, wall stress and $CD68^+$ cell activity to be even greater in vessels that dissect and especially those that rupture (approx. 10% of those that dissect). Finally, we recently reported that increased smooth muscle contractility can stress shield an otherwise vulnerable wall [30]. Albeit not shown, we confirmed weak contractility in the SAA in response to AngII, consistent with the low density of AT_{1b} receptors in this region [31], which could have contributed to its dissection propensity. Among many other possible factors, material discontinuities at branches could also contribute to dissection [32], hence the early biomechanical vulnerability of the SAA likely results from a confluence of multiple mechano- and immuno-mediated factors in AngII infusion.

Recently, there has been an increased focus on aneurysms in the ATA following AngII infusion in the $ApoE^{-/-}$ mouse [16,33]. One distinctive mechanical feature manifested in this region—circumferential material stiffness increased many-fold and remained elevated (figures 1*f* and 5*e*, electronic supplementary material, table S2A). That is, in contrast to early increases in circumferential stiffness (which one expects with increasing pressure and initial delays in collagen deposition) in the DTA, SAA and IAA that soon resolved, there was an unsuccessful attempt by intramural cells to restore this stiffness in the ATA alone. Importantly, circumferential stiffness otherwise tends to be well maintained across species under normal conditions [34] and across diverse genetic mutations that lead to mild vascular phenotypes [35,36]. That is, there is normally a strong mechanobiological control of the homeostatic mechanical state even under altered loading [23], likely accomplished via the degradation of overstretched native matrix and incorporation of new matrix having a preferred deposition stretch [27]. In contrast, our finding for the ATA is consistent with the recent observation that increased circumferential stiffness both precedes and associates with ascending aortic aneurysms in a $Fbn1^{mgR/mgR}$ mouse model of Marfan syndrome [37]. It is not clear why intramural cells of the ATA alone were unable to maintain the intrinsic circumferential material stiffness in AngII infusion, but this inability also manifested in normal ageing (figure 5). Perhaps this distinctive feature relates to a prior finding that we confirmed; namely, that the ATA alone exhibits smooth muscle cell hyperplasia (not hypertrophy) in response to AngII infusion (electronic supplementary material, figure S8A) [38]. There is motivation to determine whether an intrinsic phenotypic difference explains this distinct biomechanical behaviour and subsequent aneurysmal propensity. Finally, the ATA alone exhibited fragmented elastic fibres, which also contribute to aneurysmal dilatation [27].

Albeit observed in the SAA (3.7-fold increase in unloaded adventitial cross-sectional area at 28 days of AngII infusion) and ATA (5.5-fold increase), over-thickening of the adventitia was most prominent in the DTA (7.3-fold increase), which alone experienced significant ($p < 0.01$) reductions in circumferential wall stress at 28 days. Notwithstanding an initial increase over the first 14 days, circumferential stiffness was nevertheless well maintained and restored near baseline values at 21 and 28 days in the DTA (figure 1*f*, electronic supplementary material, table S2B). Biaxial stresses and stored energy similarly increased, then returned toward baseline levels over the first 14 days, the period during which blood pressure was increasing. Hence, the precipitous decreases in wall stress and energy storage coincided with the dramatic thickening of the wall, particularly in the adventitia (figure 2*a*,*c*,*g*). Importantly, these changes at 21+ days also coincided with marked increases in $CD45^+$ and $CD3^+$ cells in the adventitia (figure 3*d*,*e*, electronic supplementary material, table S4B). The important role of T-cells in inflammation-mediated DTA stiffening has been demonstrated in that exuberant adventitial deposition of collagen following AngII infusion is eliminated in male $Rag1^{-/-}$ mice but restored upon adoptive transfer of T-cells [20,39]. Consistent with results from other regions, our time course data show further that inflammation-mediated matrix deposition follows, rather than precedes, mechanically mediated changes (figure 4*c*,*d*); moreover, it is this excessive inflammatory mediated matrix deposition that appears mechanically maladaptive and ultimately compromises aortic function. For example, a decrease in energy storage can result from mechanical damage to or proteolytic degradation of the energy storing elastic fibres and/or a reduced ability of the wall to deform due to increased adventitial collagen deposition. The latter was likely the cause in all regions save the ATA where both factors played a role (electronic supplementary material, figure S6). Finally, the long-term persistence of biomechanical changes in the DTA (e.g. reduced stresses and stored energy; figure 5*c*,*d*,*h*) following a 7-month reduction in blood pressure (electronic supplementary material, figure S1) suggests that reverse remodelling typically occurs extremely slowly, if at all. Reversal of aortic stiffness in ageing and hypertension remains an important but challenging clinical goal [40].

Despite exposure to a dramatic increase in blood pressure and exogenous AngII, the IAA exhibited relatively modest changes in composition and mechanics over the 28-day hypertensive period. Toward this end, note that mechanoadaptive remodelling in hypertension with preserved cardiac output suggests a linear relationship between the change in thickness and the change in systolic pressure, whereby the wall should thicken by the same factor as the increase in blood pressure

(i.e. systolic wall thickness $h \rightarrow \gamma h^{0d}$ where $\gamma = P_{sys}/P^{0d}_{sys}$ and superscript 0d denotes baseline values at day 0) [21]. Thus, comparisons between relative thickness and systolic pressure can be used to assess region-specific mechanoadaptation over time. Importantly, comparing the systolic pressure ratio γ at 0, 4, 7, 14, 21 and 28 days (with $\gamma = 1.00$, 1.39, 1.50, 1.62, 1.65 and 1.67; electronic supplementary material, table S1) to the fold-increase in IAA wall thickness at these same times (e.g. 1.00-, 1.13-, 1.28-, 1.59-, 1.66- and 1.66-fold; electronic supplementary material, table S2D) reveals that the thickening was initially delayed, but then mechanically optimal (figure 4*e*,*f*). In contrast, the increase in DTA wall thickness was 1.00-, 1.05-, 1.19-, 1.62-, 3.38- and 3.86-fold for these same times, thus revealing a marked loss of mechanoadaptivity at days 21 and 28 after achieving a near optimal level at 14 days. It is not clear why the IAA alone was able to adapt optimally, but three issues merit consideration. First, the normal IAA has the greatest collagen : elastin ratio (figure 2*e*) and the additional collagen may better limit rapidly increasing pressure-induced distensions that increase wall stress (with mean circumferential wall stress $= Pa/h$, where a is the luminal radius) [41]. Second, the pulse pressure could be greater (augmented) in induced hypertension in the more proximal regions, thus increasing the mechanical stimulus for remodelling (noting that pressures were measured by tail-cuff and thus represent values closest to the IAA). Third, the IAA has the highest density of AT_{1b} receptors along the aorta [31], which may allow the smooth muscle cells to contract against the elevated pressures induced by exogenous AngII and thereby reduce the mean wall stress; albeit not shown, we confirmed that the IAA exhibits the strongest contraction to AngII of the four regions. Indeed, this possibility supports an earlier theoretical prediction that increased smooth muscle tone reduces wall stress at a given pressure [42]. In all three cases, the mechanical stimulus (e.g. changes in stress from baseline) could be modulated below levels that lead to the maladaptive remodelling seen in the other regions (figures 1*d*,*e* and 4*e*,*f*). There is a need for additional experimental work and fluid–solid interaction simulations to test these hypotheses.

Notwithstanding the mechanoadaptation of the IAA over 28 days of AngII infusion, there may have been an 'atherosclerotic priming' of this region, possibly due to the increased MMP-2 and -12 expression that facilitated early balanced matrix turnover (figure 3*a*,*b*, electronic supplementary material, table S5D), such that a nearly occlusive infrarenal neointima developed in all three mice studied 224 days after pump implantation. While all AngII-treated vessels showed some neointimal development by 224 days, the cross-sectional percentage was most pronounced in the IAA (figure 5*i*–*p* and electronic supplementary material, figure S5D–L and table S4). Noting that the SAA likely dissected within the first week of AngII infusion in these mice [28], it is possible that a thrombotic lesion proximal to the IAA could have contributed to the remarkable neointimal development by releasing soluble factors into the blood that advected downstream. Of course, oxidative stress associated with early exposure to AngII, combined with ageing to approximately 1 year, may lead to increased endothelial dysfunction [43] and thereby may contribute to excessive neointimal formation. These possibilities demand future studies focusing on inflammation and haemodynamics [29] and further emphasize the need for a systematic (fluid–solid biochemomechanical) study of global disease progression with the potential for regional interactions, not just a singular focus on one region or pathology.

Finally, the age-matched control group in the long-term study provided some information on regional differences due to ageing alone in the male $ApoE^{-/-}$ mouse. Although the aged ATA, DTA and IAA experienced a reduced distensibility in the face of modest increases in blood pressure (from $112 \pm 4/80 \pm 3$ mmHg to $138 \pm 5/105 \pm 6$ mmHg; electronic supplementary material, figure S1 and table S1), neither the DTA nor the IAA experienced any significant change in mechanical properties, save slight increases in axial stiffness ($p > 0.05$; figure 5*f*). In contrast, the normally aged ATA exhibited both a reduced axial stretch and a reduced ability to store energy ($p < 0.05$; figure 5*b*,*h*). Storing elastic energy is the primary mechanical function of large arteries, and is of particular importance in the ATA as it may contribute directly to left ventricular function. Albeit not examined here, loss of ATA functionality could increase the propensity for age-related diastolic dysfunction. The relationship between ageing and ventricular–vascular coupling in the context of ATA function demands future study. Finally, although none of the aged ATAs were aneurysmal (mean dilatation approx. 8%), the intramural cells were again unable to maintain circumferential stiffness near normal values (figure 5*e*), hence suggesting that ageing alone could predispose the ATA to dilatation, at least in male $ApoE^{-/-}$ mice, particularly given a second insult such as hypertension.

5. Conclusion

Increased central artery stiffness is an important initiator and indicator of cardiovascular, neurovascular and renovascular disease [8,9]. The present data show, for the first time, that adventitial inflammation leading to maladaptive structural stiffening follows, rather than precedes, a blood pressure-driven mechanical adaptation to increased wall stresses, even in a hypertensive model that uses an exogenous pro-inflammatory stimulant. In particular, the time course of remodelling (figures 1–3) and associated mechanoinflammatory correlations (figure 4) are consistent with: (i) an early rise in blood pressure increasing medial stress [41] and resulting in adaptive smooth muscle hyperplasia in the ATA or hypertrophy in the DTA, SAA and IAA (figure 2 and electronic supplementary material, figure S8), with modest medial and adventitial deposition of matrix (figure 2 and electronic supplementary material, figure S5A–D), and (ii) a continued marked rise in pressure increasing adventitial wall stress [41] in the ATA, and especially the SAA and DTA, that stimulates inflammatory cell recruitment along with maladaptive matrix degradation and exuberant deposition in the adventitia, the evolving balance of which dictates the fate of each affected region. The relationships among blood pressure, inflammation, and wall mechanics in the context of this study are summarized in figure 6. Clearly, controlling inflammation should be pursued if we wish to decrease the insidious positive feedback effects of maladaptive aortic stiffening [8,9].

Advances in medical imaging and medical genetics have led to an increase in the number of diagnosed ascending thoracic aneurysms, for which hypertension is a key risk factor [44–46]. The present study supports findings from multiple mouse models [37,47] showing that intramural cells within the ascending aorta are uniquely unable to control

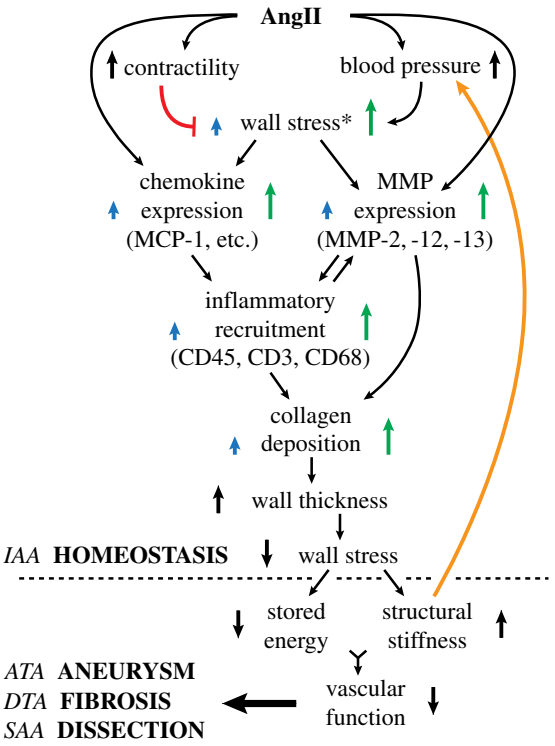

Figure 6. Schematic representation of AngII mediated aortic remodelling. Early mechanical changes (pressure- and contractility-induced increases in wall stress) drive a later inflammatory response, with positive feedback (orange line) between structural stiffness and blood pressure. Common pathways can yet result in regional differences as revealed by the mechano-adaptive response in the IAA and different maladaptive (aneurysmal propensity, fibrosis, dissection propensity) responses in the other three regions. Mechano-biological and immuno-biological responses serve as central nodes that govern regional differences. Note: a red line denotes negative feedback; blue arrows represent effects on the media and green arrows represent the more pronounced effects on the adventitia. Superscript * indicates findings from references [11] and [41].

circumferential stiffness and this contributes to aneurysmal propensity. There should be more attention directed to understanding the dysfunctional mechanobiology in this condition [23,46]. Aortic dissections are lethal conditions, with current dogma suggesting that pathogenesis progresses from an initial intimal defect. The present data support recent evidence that dissections may instead result, in part, from intramural defects [30,48], specifically suggesting that a transient imbalance in the turnover of structurally supportive collagen and/or the lack of protective smooth muscle contractility can exacerbate structural vulnerabilities. There is, therefore, a need to focus on mechanisms underlying the formation of intramural defects, not just those associated with the development of an intimal flap. Moreover, although smooth muscle contractility may be greater in the murine than the human aorta, the stress-regulating role of smooth muscle demands more attention.

Aortic ageing is a leading risk factor for myriad diseases [49,50]. The present data, for modest murine ageing to approximately 1 year, reveal a preferential loss of energy storage capability in the ATA in male $ApoE^{-/-}$ mice on a normal laboratory diet. This reduction in energy storage could increase the risk of diastolic dysfunction via the reduction of aortic restoring forces during diastolic filling. There is, therefore, a need for more quantitative assessments of ventricular–vascular coupling in terms of the wall mechanics, not just the haemodynamics.

Finally, the common clinical metric of distensibility proved unrevealing of any regional disease condition or regional propensity to disease. A greater understanding of differential regional aortic disease demands more focus on intrinsic mechanical properties such as circumferential material stiffness and elastic energy storage as well as greater attention to roles of regional mechano- and immuno-biological responses that control local remodelling.

Data accessibility. Spatio-temporal data on geometric metrics, material parameters and inflammatory information are provided in the electronic supplementary material.

Authors' contributions. M.R.B., D.G.H. and J.D.H. designed the project; M.R.B. and R.K. performed the experiments; M.R.B., R.K. and A.J.W. analysed the data; M.R.B., R.K., D.G.H. and J.D.H. interpreted the results; M.R.B. and J.D.H. drafted the paper and all authors edited and approved the final version.

Competing interests. We declare no competing interests.

Funding. This work was supported, in part, by grants from the US National Institutes of Health: R01 HL086418, R01 HL105297 and U01 HL116323 (to J.D.H.) and MSTP T32 GM07205 (to R.K.).

Acknowledgements. We thank Professor George Tellides and Dr Alex Caulk, both of Yale University, for thoughtful feedback on this study.

References

1. Mehta PK, Griendling KK. 2007 Angiotensin II cell signaling: physiological and pathological effects in the cardiovascular system. *Am. J. Physiol. Cell Physiol.* **292**, C82–C97. (doi:10.1152/ajpcell.00287.2006)
2. Unger T. 2002 The role of the renin–angiotensin system in the development of cardiovascular disease. *Am. J. Cardiol.* **89**, 3A–9A; discussion 10A. (doi:10.1016/S0002-9149(01)02321-9)
3. Van Thiel BS, Van Der Pluijm I, Te Riet L, Essers J, Danser AHJ. 2015 The renin–angiotensin system and its involvement in vascular disease. *Eur. J. Pharmacol.* **763**, 3–14. (doi:10.1016/j.ejphar.2015.03.090)
4. Daugherty A, Manning MW, Cassis LA. 2000 Angiotensin II promotes atherosclerotic lesions and aneurysms in apolipoprotein E-deficient mice. *J. Clin. Invest.* **105**, 1605–1612. (doi:10.1172/JCI7818)
5. Weiss D, Kools JJ, Taylor WR. 2001 Angiotensin II-induced hypertension accelerates the development of atherosclerosis in apoE-deficient mice. *Circulation* **103**, 448–454. (doi:10.1161/01.CIR.103.3.448)
6. Louis H *et al.* 2007 Role of alpha1beta1-integrin in arterial stiffness and angiotensin-induced arterial wall hypertrophy in mice. *Am. J. Physiol. Heart Circ. Physiol.* **293**, H2597–H2604. (doi:10.1152/ajpheart.00299.2007)
7. Wang Y *et al.* 2010 TGF-beta activity protects against inflammatory aortic aneurysm progression and complications in angiotensin II-infused mice. *J. Clin. Invest.* **120**, 422–432. (doi:10.1172/JCI38136)
8. Laurent S, Boutouyrie P. 2015 The structural factor of hypertension: large and small artery alterations. *Circ. Res.* **116**, 1007–1021. (doi:10.1161/CIRCRESAHA.116.303596)
9. Humphrey JD, Harrison DG, Figueroa CA, Lacolley P, Laurent S. 2016 Central artery stiffness in hypertension and aging a problem with cause and consequence. *Circ. Res.* **118**, 379–381. (doi:10.1161/CIRCRESAHA.115.307722)
10. Ferruzzi J, Bersi MR, Humphrey JD. 2013 Biomechanical phenotyping of central arteries in health and disease: advantages of and methods for

murine models. *Ann. Biomed. Eng.* **41**, 1311–1330. (doi:10.1007/s10439-013-0799-1)

11. Bersi MR, Bellini C, Wu J, Montaniel KRC, Harrison DG, Humphrey JD. 2016 Excessive adventitial remodeling leads to early aortic maladaptation in angiotensin-induced hypertension. *Hypertension* **67**, 890–896. (doi:10.1161/HYPERTENSIONAHA.115.06262)
12. Wolinsky H, Glagov S. 1967 A lamellar unit of aortic medial structure and function in mammals. *Circ. Res.* **20**, 99–111. (doi:10.1161/01.RES.20.1.99)
13. Capers Q, Alexander RW, Lou P, Hector De Leon P, Wilcox JN, Ishizaka N, Howard AB, Taylor WR. 1997 Monocyte chemoattractant protein-1 expression in aortic tissues of hypertensive rats. *Hypertension* **30**, 1397–1402. (doi:10.1161/01.HYP.30.6.1397)
14. Wagenseil JE, Mecham RP. 2009 Vascular extracellular matrix and arterial mechanics. *Physiol. Rev.* **89**, 957–989. (doi:10.1152/physrev.00041.2008)
15. Ferruzzi J, Bersi MR, Mecham RP, Ramirez F, Yanagisawa H, Tellides G, Humphrey JD. 2016 Loss of elastic fiber integrity compromises common carotid artery function: implications for vascular aging. *Artery Res.* **14**, 41–52. (doi:10.1016/j.artres.2016.04.001)
16. Trachet B *et al.* 2016 Ascending aortic aneurysm in angiotensin II-infused mice: formation, progression, and the role of focal dissections. *Arterioscler. Thromb. Vasc. Biol.* **36**, 673–681. (doi:10.1161/ATVBAHA.116.307211)
17. Li Q, Muragaki Y, Hatamura I, Ueno H, Ooshima A. 1998 Stretch-induced collagen synthesis in cultured smooth muscle cells from rabbit aortic media and a possible involvement of angiotensin II and transforming growth factor-beta. *J. Vasc. Res.* **35**, 93–103. (doi:10.1159/000025570)
18. O'Callaghan CJ, Williams B. 2000 Mechanical strain-induced extracellular matrix production by human vascular smooth muscle cells: role of TGF-beta(1). *Hypertension* **36**, 319–324. (doi:10.1161/01.HYP.36.3.319)
19. Browatzki M, Larsen D, Pfeiffer CAH, Gehrke SG, Schmidt J, Kranzhöfer A, Katus HA, Kranzhöfer R. 2005 Angiotensin II stimulates matrix metalloproteinase secretion in human vascular smooth muscle cells via nuclear factor-kappaB and activator protein 1 in a redox-sensitive manner. *J. Vasc. Res.* **42**, 415–423. (doi:10.1159/000087451)
20. Wu J, Thabet SR, Kirabo A, Trott DW, Saleh MA, Xiao L, Madhur MS, Chen W, Harrison DG. 2014 Inflammation and mechanical stretch promote aortic stiffening in hypertension through activation of p38 mitogen-activated protein kinase. *Circ. Res.* **114**, 616–625. (doi:10.1161/CIRCRESAHA.114.302157)
21. Humphrey JD. 2008 Mechanisms of arterial remodeling in hypertension: coupled roles of wall shear and intramural stress. *Hypertension* **52**, 195–200. (doi:10.1161/HYPERTENSIONAHA.107.103440)
22. Eberth JF, Popovic N, Gresham VC, Wilson E, Humphrey JD. 2010 Time course of carotid artery growth and remodeling in response to altered pulsatility. *Am. J. Physiol. Heart Circ. Physiol.* **299**, H1875–H1883. (doi:10.1152/ajpheart.00872.2009)
23. Humphrey JD, Dufresne ER, Schwartz MA. 2014 Mechanotransduction and extracellular matrix homeostasis. *Nat. Rev. Mol. Cell Biol.* **15**, 802–812. (doi:10.1038/nrm3896)
24. Bardy N, Merval R, Benessiano J, Samuel JL, Tedgui A. 1996 Pressure and angiotensin II synergistically induce aortic fibronectin expression in organ culture model of rabbit aorta. Evidence for a pressure-induced tissue renin–angiotensin system. *Circ. Res.* **79**, 70–78. (doi:10.1161/01.RES.79.1.70)
25. Lehoux S, Lemarié CA, Esposito B, Lijnen HR, Tedgui A. 2004 Pressure-induced matrix metalloproteinase-9 contributes to early hypertensive remodeling. *Circulation* **109**, 1041–1047. (doi:10.1161/01.CIR.0000115521.95662.7A)
26. Valentín A, Humphrey JD. 2009 Parameter sensitivity study of a constrained mixture model of arterial growth and remodeling. *J. Biomech. Eng.* **131**, 101006. (doi:10.1115/1.3192144)
27. Wilson JS, Baek S, Humphrey JD. 2013 Parametric study of effects of collagen turnover on the natural history of abdominal aortic aneurysms. *Proc. Math. Phys. Eng. Sci.* **469**, 20120556. (doi:10.1098/rspa.2012.0556)
28. Saraff K, Babamusta F, Cassis LA, Daugherty A. 2003 Aortic dissection precedes formation of aneurysms and atherosclerosis in angiotensin II-infused, apolipoprotein E-deficient mice. *Arterioscler. Thromb. Vasc. Biol.* **23**, 1621–1626. (doi:10.1161/01.ATV.0000085631.76095.64)
29. Phillips EH, Di Achille P, Bersi MR, Humphrey JD, Goergen CJ. 2017 Multi-modality imaging enables detailed hemodynamic simulations in dissecting aneurysms in mice. *IEEE Trans. Med. Imaging* **36**, 1297–1305. (doi:10.1109/TMI.2017.2664799)
30. Ferruzzi J, Murtada S, Li G, Jiao Y, Uman S, Ting MYL, Tellides G, Humphrey JD. 2016 Pharmacologically improved contractility protects against aortic dissection in mice with disrupted transforming growth factor-beta signaling despite compromised extracellular matrix properties. *Arterioscler. Thromb. Vasc. Biol.* **36**, 919–927. (doi:10.1161/ATVBAHA.116.307436)
31. Poduri A, Owens AP, Howatt DA, Moorleghen JJ, Balakrishnan A, Cassis LA, Daugherty A, Zirlik A. 2012 Regional variation in aortic AT1b Receptor mRNA abundance is associated with contractility but unrelated to atherosclerosis and aortic aneurysms. *PLoS One* **7**, e48462. (doi:10.1371/journal.pone.0048462)
32. Trachet B *et al.* 2014 Dissecting abdominal aortic aneurysm in Ang II-infused mice: suprarenal branch ruptures and apparent luminal dilatation. *Cardiovasc. Res.* **105**, 213–222. (doi:10.1093/cvr/cvu257)
33. Rateri DL *et al.* 2014 Angiotensin II induces region-specific medial disruption during evolution of ascending aortic aneurysms. *Am. J. Pathol.* **184**, 2586–2595. (doi:10.1016/j.ajpath.2014.05.014)
34. Shadwick RE. 1999 Mechanical design in arteries. *J. Exp. Biol.* **202**, 3305–3313.
35. Bersi MR, Ferruzzi J, Eberth JF, Gleason RL, Humphrey JD. 2014 Consistent biomechanical phenotyping of common carotid arteries from seven genetic, pharmacological, and surgical mouse models. *Ann. Biomed. Eng.* **42**, 1207–1223. (doi:10.1007/s10439-014-0988-6)
36. Ferruzzi J, Bersi MR, Uman S, Yanagisawa H, Humphrey JD. 2015 Decreased elastic energy storage, not increased material stiffness, characterizes central artery dysfunction in fibulin-5 deficiency independent of sex. *J. Biomech. Eng.* **137**, 031007. (doi:10.1115/1.4029431)
37. Bellini C, Korneva A, Zilberberg L, Ramirez F, Rifkin DB, Humphrey JD. 2016 Differential ascending and descending aortic mechanics parallel aneurysmal propensity in a mouse model of Marfan syndrome. *J. Biomech.* **49**, 2383–2389. (doi:10.1016/j.jbiomech.2015.11.059)
38. Owens AP, Subramanian V, Moorleghen JJ, Guo Z, McNamara CA, Cassis LA, Daugherty A. 2010 Angiotensin II induces a region-specific hyperplasia of the ascending aorta through regulation of inhibitor of differentiation 3. *Circ. Res.* **106**, 611–619. (doi:10.1161/CIRCRESAHA.109.212837)
39. Guzik TJ *et al.* 2007 Role of the T cell in the genesis of angiotensin II induced hypertension and vascular dysfunction. *J. Exp. Med.* **204**, 2449–2460. (doi:10.1084/jem.20070657)
40. Nilsson PM, Boutouyrie P, Laurent S. 2009 Vascular aging: a tale of EVA and ADAM in cardiovascular risk assessment and prevention. *Hypertens* **54**, 3–10. (doi:10.1161/HYPERTENSIONAHA.109.129114)
41. Bellini C, Ferruzzi J, Roccabianca S, Di Martino ES, Humphrey JD. 2014 A microstructurally motivated model of arterial wall mechanics with mechanobiological implications. *Ann. Biomed. Eng.* **42**, 488–502. (doi:10.1007/s10439-013-0928-x)
42. Humphrey JD, Wilson E. 2003 A potential role of smooth muscle tone in early hypertension: a theoretical study. *J. Biomech.* **36**, 1595–1601. (doi:10.1016/S0021-9290(03)00178-7)
43. Cai H, Harrison DG. 2000 Endothelial dysfunction in cardiovascular diseases: the role of oxidant stress. *Circ. Res.* **87**, 840–844. (doi:10.1161/01.RES.87.10.840)
44. Ince H, Nienaber CA. 2007 Etiology, pathogenesis and management of thoracic aortic aneurysm. *Nat. Clin. Pract. Cardiovasc. Med.* **4**, 418–427. (doi:10.1038/ncpcardio0937)
45. Milewicz DM, Guo D-C, Tran-Fadulu V, Lafont AL, Papke CL, Inamoto S, Kwartler CS, Pannu H. 2008 Genetic basis of thoracic aortic aneurysms and dissections: focus on smooth muscle cell contractile dysfunction. *Annu. Rev. Genomics Hum. Genet.* **9**, 283–302. (doi:10.1146/annurev.genom.8.080706.092303)
46. Humphrey JD, Schwartz MA, Tellides G, Milewicz DM. 2015 Role of mechanotransduction in vascular biology: focus on thoracic aortic aneurysms and dissections. *Circ. Res.* **116**, 1448–1461. (doi:10.1161/CIRCRESAHA.114.304936)

47. Bellini C *et al.* 2017 Comparison of 10 murine models reveals a distinct biomechanical phenotype in thoracic aortic aneurysms. *J. R. Soc. Interface* **14**, 20161036. (doi:10.1098/rsif.2016.1036)
48. Roccabianca S, Ateshian GA, Humphrey JD. 2014 Biomechanical roles of medial pooling of glycosaminoglycans in thoracic aortic dissection. *Biomech. Model. Mechanobiol.* **13**, 13–25. (doi:10.1007/s10237-013-0482-3)
49. Lakatta EG, Wang M, Najjar SS. 2009 Arterial aging and subclinical arterial disease are fundamentally intertwined at macroscopic and molecular levels. *Med. Clin. North Am.* **93**, 583–604. (doi:10.1016/j.mcna.2009.02.008)
50. Safar ME. 2010 Arterial aging—hemodynamic changes and therapeutic options. *Nat. Rev. Cardiol.* **7**, 442–449. (doi:10.1038/nrcardio.2010.96)